Medicon Engineering Themes
Volume 7 Issue 3 September 2024
Article Type: Research Article
ISSN: 2834-7218

Novel Technique for Generation of X-ray Based on Molecular Quantum Harmonic Oscillator and Subsequent Application in Determination of Carcinoma of Lungs and Breast Cells Using Gold Nanowire Network

Sachindeb Jana[1]*, Kisalaya Chakrabarti[1] and Angsuman Sarkar[2]

[1]*Haldia Institute of Technology, West Bengal, India*

[2]*Kalyani Government Engineering College, West Bengal, India*

***Corresponding Author:** Sachindeb Jana, Haldia Institute of Technology, West Bengal, India.

Received: August 30, 2024; **Published:** September 11, 2024

Abstract

The X-ray is a fantastic invention that has found widespread use in the medical area and as a metal detector, among other things. However, because the conventional X-ray generating technique requires a high voltage of several kilovolts, it is expensive. Here, we've presented a reliable technique that makes use of quantum technology to produce X-rays with just a few volts. In addition, we have implemented an X-ray method for the identification of lung and breast cancer. The next step is precisely positioning gold nanowires for tailored drug delivery. The interaction of light with metal nanoparticles has been studied for a very long time, both theoretically and experimentally. Silver and gold nanoparticles, which usually have sizes between 5 and 150 nm, are very interesting because they have the ability to modify their binding affinity. This means that the formulation of the nanoparticles may be perfectly matched to a particular type of cancer by excitation with the resonance of the generated X-ray spectrum range. On the other hand, when these particles are arranged as grating elements in a gold nanowire network structure (AuNW), several interesting occurrences take place.

Keywords: Molecular FCN; QHO; X-ray; AuNW; Targeted drug delivery

Introduction

Wilhelm Röntgen's discovery of the X-ray was one of the most significant discoveries of the 19th century. At that time, the radiation was referred to as X-rays or X-radiation and was an unidentified type. According to current convention, an X-ray tube is necessary for X-ray production. It is a vacuum tube that accelerates electrons by using a high voltage from a cathode plate. When these fast-moving electrons collide with a metal anode, they release X-rays [1].

With a production efficiency of just 1%, the current X-ray generation technology is ineffective. To generate the necessary flux of X-rays, the procedure uses a sizable amount of power [2]. A three to single phase transformer is used with a 440V AC, 50/60 Hz supply in the digital X-ray generator. Here, the production of X-rays results in the generation of about 80 KVA of power. The majority of this is wastage as heat that the tube absorbs. Because of its construction, the current X-ray tube is able to dissipate extra heat. When producing X-rays, energy and power loss are of major concerns, and there are numerous research projects underway worldwide [3]. Since the current technique generates X-ray at a temperature of about 25000 Celsius, a cooling system is necessary. The Us patent [4] reveals enhancement of optical portion of an X-ray radiographic or same kind of optical imaging system by enhancing the part of light emitted from an X-ray converter screen which is projected into the collection cone of an objective lens. In addition, this lessens the impact of light leaving the X-ray converter screen—which is made up of a diffuse phosphor screen—in a direction that the lens is

unable to catch. In other words, the innovation lessens the quantity of light that the imager allows to scatter. This optical system may generate an image that is brighter and has better contrast than it could have before. Another US patent [5] described about the new model of X-ray generation. An electron emitter for an X-ray tube and an X-ray image capture system are the subject of this invention. This invention also relates to a computer program element designed to control an object acquisition method (such as transmission radiography using X-rays), a computer-readable medium that contains the computer program element stored on it. In the patent [6] the inventor claimed an X-ray emission electron source related to nano structures as emitters and self-aligned nano-scaled gate formation for the control of low voltage. The most promising substance among them all seems to be carbon nanotubes (CNTs). Several studies have documented the beneficial emission characteristics of carbon nanotubes. It can conduct a current up to 500 nA per tube and has a low electron energy spread with a threshold field as low as 1 to 2×106 V/m. It is the perfect field emitter due to its exceptional high electrical and thermal conductivity, robust chemical stability, and mechanical durability. One more patent [7] claimed about the invention of x-ray imaging devices ,more precisely an X-ray tube with increased control of electron beam emission. Another US patent [8] relates to an X-ray system and the utilization of an X-ray generator in a minimum of one Cathode ray Tube system with an electron scattering element.

All of these above inventors used conventional method of X-ray generation where X-ray tube, anode and cathod elements are commom with some additional arrangements. First time ever we are proposed the new era of generating X-ray using Quantum technology. Our proposed method is on the working pring principle of Quantum Harmonic Oscillator alongwith Molecular Field Coupled Nanocomputing, where the difference of energy levels are of same eV which caters the need. Using the quantum dot cellular automata [9] paradigm, X-ray waves can be produced with very little power consumption—about one watt and very little supply voltage, between 2 and 2.81 Vrms [10]. The technique for producing X-ray waves from QCA units using Quantum Harmonic Oscillator(QHO) [11] is the subject of the current invention.

Molecular Field Coupled Nanocomputing

Our proposed article is going to focus on X-ray generation using the energy criteria of Quantum harmonic Oscillator which works on the Quantum cellular Automata (QCA) technology. One of the drawback of QCA is that those circuit implemented by QCA can not deliver output satisfactorily after the temperature10K. Working below temperature of 10K is quite difficult. To avoid this problem various new technologies have been discussed to execute QCA like metallic, magnetic, and molecular execution. The most promising of them is molecular Field-Coupled Nanocomputing (FCN) [12], which is expected to provide very high device density and very high frequency operations at room temperature. In specifics, the molecular FCN [13] paradigm encodes information in the charge distribution of molecules to construct computational electronic devices. Typically, a more generic electron cloud that aggregates at certain molecular locations to form QCA quantum dots takes the role of the electrons of the QCA paradigm.

Using a few molecules to create a cell—known as the “molecular FCN”—is one method of technologically implemention of QCA paradigm. The molecules of the same cell display two opposite dipole moments (m1 and m2), as shown in Fig. 1(b). These molecules encode the logical states ‘0’ and ‘1’ and replicate the existence of two charges in two of the four quantum-dots of QCA cells. Two additional benefits come from applying the paradigm to molecules: we can create extremely small devices which operate at room temperature.

As seen in Fig. 1(b), in addition to the fundamental use of the first two logic states, a third state called “NULL” is employed to encode absence of information. Adiabatic and pipelined propagation require the “NULL” state, which is achieved by adding an external electric field known as the clock field. In fact, as Fig. 1c illustrates, information can be propagated over FCN wires by aligning several molecular cells. The information can be steered by partitioning the molecular wire within clock zones, which are consecutively triggered by the clock field. This eventually prevents information anomalies during propagation and reduces power consumption. Logic operations and connections can be implemented by arranging cells into ordered structures.

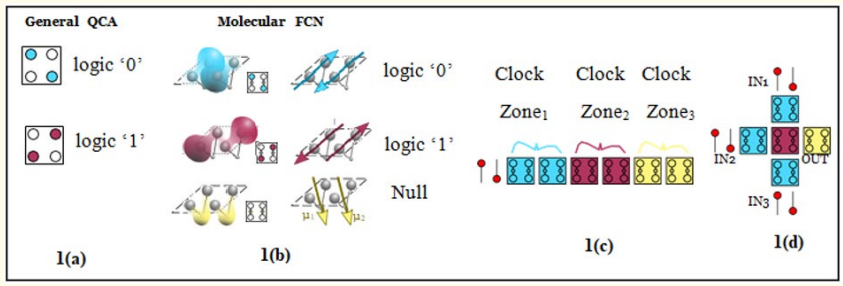

Figure 1: Information encoding, propagation, and elaboration. (a) In the QCA paradigm, information is encoded as two electrons placed on the antipodal quantum dots of a QCA cell; (b) Information in the molecular FCN, information is encoded as two adjacent molecules' charge distribution and the resulting anti symmetric dipole moments, μ1 and μ2, arranged to resemble a QCA cell configuration; (c) Molecular FCN wire: six molecular cells separated into three clock zones are used to propagate the information; (d) Molecular FCN majority voter (obtained from [12]).

The Majority Voter (MV) with three inputs is depicted in Fig. 1(d). The fanout gate, which is one of the potential devices, duplicates the data encoded by the input cell to three output wires (Fig. 2(a)). The inverter, another type of elementary logic gate, has two distinct layouts in the literature: the double-branch inverter depicted in Fig. 2(c) and the single-branch inverter illustrated in Fig. 2(b). The Aggregated Charge (AC) [14] represents a molecule's charge distribution. For example, by fitting the electrostatic potential from ab initio computation, the atomic charges of the bis-ferrocene molecule, which was ad hoc fabricated for molecular FCN computing and illustrated in Fig. 3(a), may be obtained. Because of the distinctive structural, spectroscopic, and electrochemical characteristics of ferrocene and its derivatives, a great deal of study and research has been done on them. Ferrocene oxidizes one electron reversibly at a low voltage of about 0.5 V. Ferrocene derivatives that display several ferrocene groups are being extensively investigated for use as molecular diodes due to their potential to produce mixed-valent states.

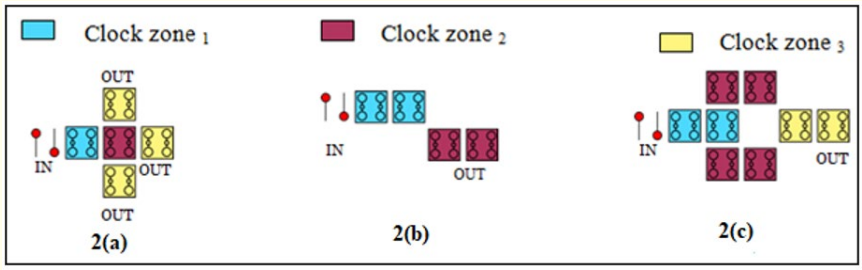

Figure 2: Layout implementing probable operations in molecular FCN. (a) The fanout: (b) the single-branch inverter (c) the double-branch inverter (obtained from [12]).

The atomic charges and functional groups shown in Fig. 3(b) allow for the derivation of the AC, which is really the total of the atomic charges that make up a molecule's functional group. Functional grouping present in the molecular FCN paradigm's are analogue to the QCA dots, as shown in Fig. 3(c). The Voltage-Aggregated Charge Transcharacteristic (VACT) [15] is obtained by relating the performance of the AC for various input voltages.

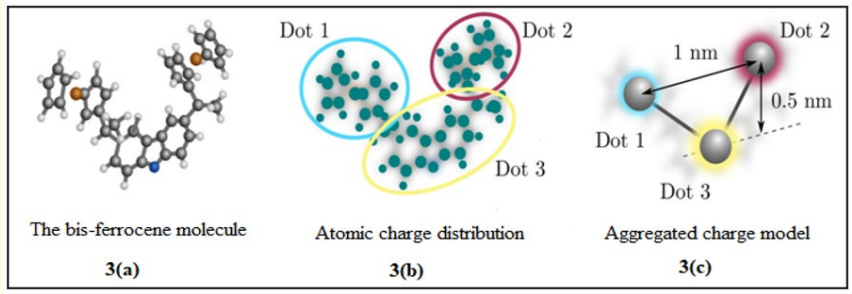

Figure 3: The Aggregated Charge model is derived using an ab initio computation. (a)Two ferrocenes and a carbazole make up the bis-ferrocene molecule. (b)The atomic charges that result from seting the electrostatic potential that the bis-ferrocene molecule generates, which can be evaluated using ab initio calculation,The circles, which stand for the group of atomic charges used to estimate the aggregated charges (c) Total charge distribution acquired by adding up the atomic charges within the designated groupings. (obtained from [12]).

Temperature dependancy of molecular Field Coupled Nanocomputing

In the following section we are aiming to establish the relationship between energy and temperature. The system energy only includes terms that describe how each cell in the wire interrelates with its closest neighbors, assuming that each cell only interacts strongly with their neighbors. The final simplified equation of the system energy (E) for wires with input value of '1', and '-1' respectively [15], has been written in equations (1) and (2) as follows:

$$E = C_1 N + C_2 S_1 + C_2 \sum_{m=1}^{N-1} S_m S_{m+1} \quad , \quad (S_0 = 1) \text{ Here, } S_1 = \pm 1 \ldots\ldots S_N = \pm 1 \qquad (1)$$

$$E = C_1 N - C_2 S_1 + C_2 \sum_{m=1}^{N-1} S_m S_{m+1} \quad , \quad (S_0 = -1), \text{ where} \qquad (2)$$

$$C_1 = \frac{e^2}{8\pi\varepsilon L}\left(\frac{1+\sqrt{1+a^2}}{\sqrt{1+a^2}}\right) \quad , \quad \left(a = \frac{d}{L}\right) \qquad (3)$$

$$C_2 = \frac{e^2}{8\pi\varepsilon L}\left(\frac{1-\sqrt{1+a^2}}{\sqrt{1+a^2}}\right), \qquad (4)$$

d =distance between dots in the cell, L = cell-cell distance and N =number of cell

Finally,

$$\langle S_N \rangle = (-1)^N \left(\frac{e^{\frac{C_2}{KT}} - e^{-\frac{C_2}{KT}}}{e^{\frac{C_2}{KT}} + e^{-\frac{C_2}{KT}}}\right)^N \quad , \quad \text{for input: '1'} \qquad (5)$$

and

$$\langle S_N \rangle = (-1)^{N-1} \left(\frac{e^{\frac{C_2}{KT}} - e^{-\frac{C_2}{KT}}}{e^{\frac{C_2}{KT}} + e^{-\frac{C_2}{KT}}}\right)^N \quad , \quad \text{for input: '-1'} \qquad (6)$$

This analytical formula allows us to investigate the link between $\langle S_N \rangle$ (expected polarization of the output cell) and several parameters like the number of cells in a wire, the distance between cells, and the operating temperature, fig. 4 shows the results of a brute-force calculation of the nearest neighbor estimates compared to temperature. fig. 5 shows the results of temperature dependence of $\langle S_N \rangle$ for many relatively long wires by Ising approximation method.

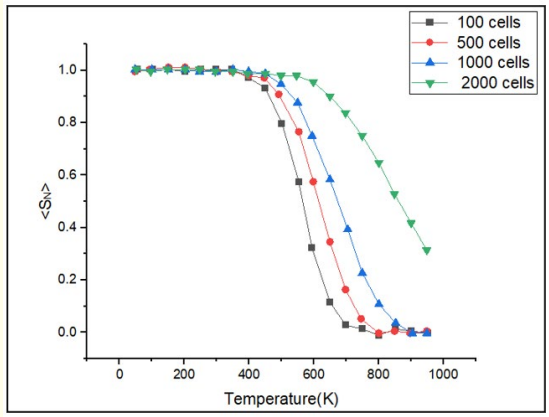

Figure 4: Ising approximation findings for semi-infinite MQCA wires. Temperature dependency of $\langle S_N \rangle$ for many relatively long wires with cell parameters $d = L = 10\ \mathring{A}$. The expected result is +1 when even numbers of two-dot cells and an input polarization value of 1 are used (Redrawn from the data retrieved from the fig. 8(a) of [15]).

From the above graph it is observable that in molecular FCN polarization of cells i.e. $\langle S_N \rangle$ is achieved up to the temperature range of 400k which is one of the criteria of X-ray generation (ambient operating temperature). We have considered 300k for plotting of wave functions and energy eigen states of quantum harmonic oscillator.

We have done a statistical analysis of the graphs shown in fig. 5(a) and 5(c),then presented the results in two new graphs 5(b) and 5(d) respectively. The half power approach is considered here for getting expected polarisation in respect to temperature range. Here σ, standard deviation obtained in the "Temperature (K)" axis correspond the value of Expected Polarization $\langle S_N \rangle$. We are considering temperature range(2σ) for which expected polarisation is above .707 or -.707 for positive or negetive polarisation respectively. From these two graphs it is clearly visible that polarisation of cells (to 1 or -1) is achieved in the temperature range of 220K to 520K (approximately) which covers the room temperature 300K.

Generation of X-ray

In quantum mechanics an operator that represents a system's entire energy, including both kinetic and potential energy, is called its Hamiltonian. Its spectrum, also known as the system's energy spectrum or its set of energy eigen values, is the range of possible results that can be obtained by measuring the total energy of the system. Because of its intimate connection to a system's energy spectrum and time-evaluation it is a fundamental formula of quantum mechanics [17].

The well known equation of Hamiltonian of a particle is:

$$\hat{H} = \frac{\hat{p}^2}{2m} + \frac{1}{2}k\hat{x}^2 = \frac{\hat{p}^2}{2m} + \frac{1}{2}m\omega^2 x^2 \quad (7)$$

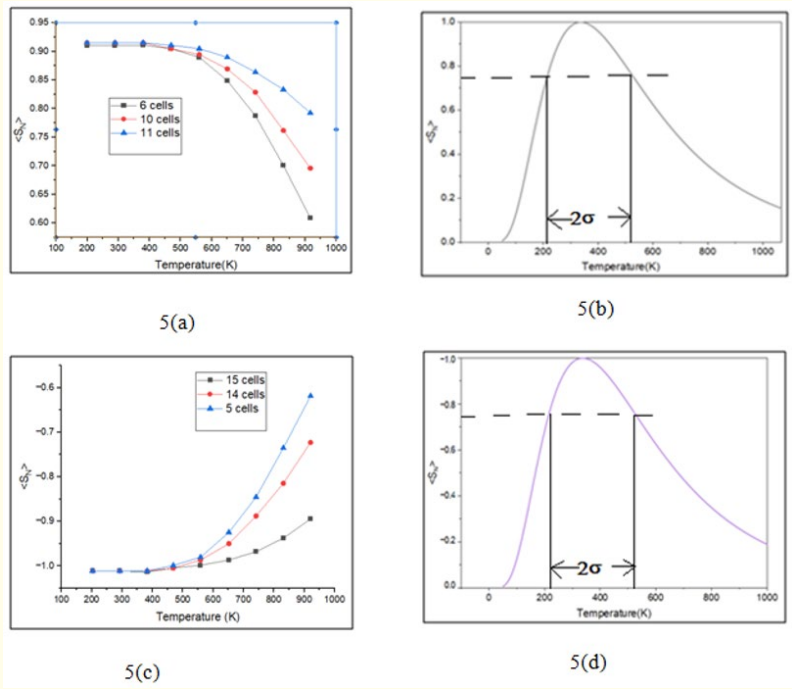

Figure 5: (a) depicts $\langle S_N \rangle$ vs. temperature dependence for multiple N-cell wires with $d = L = 10\,\mathring{A}$. The range of N is{6,10,11}. When an input polarization value of -1 is utilized, the expected output value's sign will either be +1 or -1 depending on whether the wire's total number of cells is even or odd. (Redrawn using the data retrieved from the Fig. 5(a) of [16]), (b) Statistical analysis of temperature vs. expected polarization $\langle S_N \rangle$ given in Fig. 5(a).
(c) depicts $\langle S_N \rangle$ vs. temperature dependence for multiple N-cell wires with $d = L = 10\,\mathring{A}$. The range of N is {5,14,15}. When an input polarization value of -1 is utilized, the expected output value's sign will either be +1 or -1 depending on whether the wire's total number of cells is even or odd. (Redrawn using the data retrieved from the fig. 5(a) of [16]).
(d) Statistical analysis of temperature vs. expected polarization $\langle S_N \rangle$ given in fig. (c).

Where is mass of the particle, is angular frequency can be written as $\sqrt{\frac{k}{m}}$, is force constant, $\hat{x}$ position operator, $\hat{p}$ is the momentum operator. The particle's kinetic energy is represented by the first part in the Hamiltonian, while its potential energy is represented by the second term.

The time independent Schrödinger equation is:

$$\hat{H}\,|\psi\rangle = E\,|\psi\rangle \quad (8)$$

where the solution $|\psi\rangle$ indicates the energy eigen state of that level and E indicates a real integer (which has to be calculate) that will identify an eigenvalue, or time-independent energy level.

For the wave function $\langle x\,|\psi\rangle = \psi(x)$,

$$\psi_n(x) = \frac{1}{\sqrt{2^n n!}} \left(\frac{m\omega}{\pi\hbar}\right)^{\frac{1}{4}} e^{-\frac{m\omega z^2}{2\hbar}} H_n\left(\sqrt{\frac{m\omega}{\hbar}}x\right) \quad n=0, 1, 2, 3..... \quad (9)$$

$H_n(z)$ is a polynomial of degree n called a Hermite polynomial. The first four Hermite polynomials are

$$H_0(z) = 1$$
$$H_1(z) = 2z$$
$$H_2(z) = 4z^2 - 2$$
$$H_3(z) = 8z^3 - 12z$$

Merging this expression with the time-independent Schrödinger equation gives

$$-\frac{\hbar}{2m}\frac{d^2\psi(x)}{dx^2} + \frac{1}{2}m\omega^2 x^2\psi(x) = E\psi(x) \quad (10)$$

The allowed energies are:

$$E_n = (n+\frac{1}{2})\hbar\omega$$

$$= \frac{2n+1}{2}\hbar\omega \quad n=0, 1, 2... \quad (11)$$

The energy eigen states for different values of n is shown in fig-6. $H_n(z)$ is a polynomial of degree n called a Hermite polynomial. The first four Hermite polynomials are

$$H_0(y) = 1$$
$$H_1(y) = 2y$$
$$H_2(y) = 4y^2 - 2$$
$$H_3(y) = 8y^3 - 12y$$

Below we have presented the first five waveforms of QHO plotted using the software Matlab 13.1 (considering the values of n from 1 to 5) showing the relation of eigen energies with eigen states. Vertical lines represent the traditional turning points at x=±A of a traditional particle with the same energy of a quantum oscillator in the state depicted in the picture, which indicate the classical limitations of the oscillator's motion. Pseudo codes of this plot is given in the appendix-1.

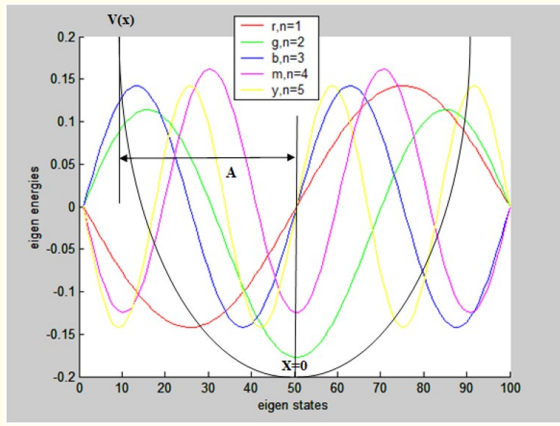

Figure 6: The quantum harmonic oscillator's first five wavefunctions.

Calculation of energy for X-ray generation

Now,

$$E_n = m\omega^2 A_n^{\,2}/2$$
$$A_n = \sqrt{\frac{2}{m\omega^2}En}$$
$$= \sqrt{\frac{2}{m\omega^2}\frac{2n+1}{2}\hbar\omega}$$
$$= \sqrt{\frac{(2n+1)}{m\omega}\hbar} \qquad (12)$$

as the quantum number n increases, the oscillator's energy and the amplitude both grow . Moreover, the permitted energy levels are uniformly spaced, in contrast to the situation of a quantum particle in a box.

$$\Delta E = E_{n+1} - E_n$$
$$= \frac{2(n+1)+1}{2}\hbar\omega - \frac{2n+1}{2}\hbar\omega \quad (13)$$

Invariably, when a particle coupled to such a system transitions from a higher-energy state to a lower-energy state, the photon that is released carries the smallest-energy quantum possible. This is consistent with Planck's theory of the energy exchanges between the cavity and the radiation barriers in the blackbody radiation problem.

The required energy for X-ray generation have to be in the range of 5×10^3 eV to 10^4 eV [18] and frequency should be in the range of 1×10^{18}Hz to 3×10^{19}Hz. Value of the ħ is 6.58×10^{-16}. Putting the values of ħ and ω, energy difference between any two consecutive energy levels is from 6.58×10^2eV to 19.74×10^3eV. But the X-ray can be generated within 10^4 eV. For that maximum frequency would be 1.52×10^{19}Hz. Applying the light energy of minimum frequency i:e 1×10^{18}Hzenergy difference is coming 6.58×10^2 eV and it is easily calculated that required energy level gap for X-ray generation would be 8,9,10,11,12,13,14,15. For maximum frequency range energy level gap will be 1 only. It is always beneficial to select (i) signal of low frequency range (ii) median value of allowable energy level gap for deviation of energy in either side from its original value. Therefore best selcted value of frequency is 1×10^{18}Hz and energy level gap 11 or 12.

Annihilation & Creation Operators

Energy analysis of quantum harmonic oscillators can be done by the use of two simultaneous operators stepwise, named Annihilation & Creation Operators. These operators are the transition between adjacent quantum harmonic oscillators' eigen states.

$$\hat{a}|n\rangle = \begin{cases} 0 & , n = 0 \\ \sqrt{n}|n-1\rangle, & otherwise \end{cases}$$
$$\hat{a}\dagger|n\rangle = \sqrt{n+1}|n+1\rangle \qquad (14)$$

Where $\hat{a} \rightarrow$lowering operator

$\hat{a}\dagger \rightarrow$ raising operator

This energy analysis is nicely represented by Fock- space energy basis. The general state as a superposition of eigen states $\{|n\rangle\}$ of Hamiltonian $\hat{H}$

$$|\Psi\rangle = \sum_{n=0}^{\infty} C_n |n\rangle, \text{ where } C_n = \langle n|\Psi\rangle \quad (15)$$

We can write the elementary vector to represent eigen states $\{|n\rangle\}$

$$|0\rangle \leftrightarrow \begin{bmatrix} 1 \\ 0 \\ 0 \\ 0 \\ . \\ . \\ . \end{bmatrix}, \quad |1\rangle \leftrightarrow \begin{bmatrix} 0 \\ 1 \\ 0 \\ 0 \\ . \\ . \\ . \end{bmatrix}, \quad |2\rangle \leftrightarrow \begin{bmatrix} 0 \\ 0 \\ 1 \\ 0 \\ . \\ . \\ . \end{bmatrix}, \quad .....$$

And the general eigen vector of representing eigen states is

$$|\Psi\rangle \leftrightarrow \begin{bmatrix} C_0 \\ C_1 \\ C_2 \\ C_3 \\ . \\ . \\ . \end{bmatrix}$$

Next step is the use of annihilation operator which works upon two factors to represent , which is the matrix representation of $\hat{a}$ in the $\{|n\rangle\}$

First factor is $\hat{a}|n\rangle = \sqrt{n}\,|n-1\rangle$ for lowering operator. Second $\hat{a}|n\rangle$ picks out the nth column of $\tilde{a}\dagger$.

$$\hat{a}|0\rangle = 0 \leftrightarrow \begin{bmatrix} 0 \\ 0 \\ 0 \\ 0 \\ . \\ . \\ . \end{bmatrix}, \quad \hat{a}|1\rangle = |0\rangle \leftrightarrow \begin{bmatrix} 1 \\ 0 \\ 0 \\ 0 \\ . \\ . \\ . \end{bmatrix}, \quad \hat{a}|2\rangle = \sqrt{2}\,|1\rangle \leftrightarrow \begin{bmatrix} 0 \\ \sqrt{2} \\ 0 \\ 0 \\ . \\ . \\ . \end{bmatrix}, \quad .....$$

Therefore general representation of $\hat{a}$ is by this matrix and the energy basis.....

$$\hat{a} = \begin{bmatrix} 0 & 1 & 0 & 0 & 0 & . & . & . \\ 0 & 0 & \sqrt{2} & 0 & 0 & . & . & . \\ 0 & 0 & 0 & \sqrt{3} & 0 & . & . & . \\ 0 & 0 & 0 & 0 & \sqrt{4} & . & . & . \\ . & . & . & . & . & . & . & . \\ . & . & . & . & . & . & . & . \\ . & . & . & . & . & . & . & . \end{bmatrix}$$

Creation Operator

Creation operator simply works on the conjugate and transpose of $\tilde{a}\dagger$ which is represented below.

$$\tilde{a} = \begin{bmatrix} 0 & 1 & 0 & 0 & 0 & . & . & . \\ 0 & 0 & \sqrt{2} & 0 & 0 & . & . & . \\ 0 & 0 & 0 & \sqrt{3} & 0 & . & . & . \\ 0 & 0 & 0 & 0 & \sqrt{4} & . & . & . \\ . & . & . & . & . & . & . & . \\ . & . & . & . & . & . & . & . \\ . & . & . & . & . & . & . & . \end{bmatrix}$$

These are energy raising operators.

Combining lowering and raising operators of energy basis are used to explain Hamiltonian:

$$\hat{H} = \hbar\omega(\hat{a}\dagger\hat{a} + \frac{1}{2}\hat{1}) \quad (16)$$

$$\hat{H} \leftrightarrow \tilde{H} = \hbar\omega(\hat{a}\dagger\tilde{a} + \frac{1}{2}\tilde{1}) \quad (17)$$

$$\tilde{H} = \frac{\hbar\grave{u}}{2}\begin{bmatrix} 1 & 0 & 0 & 0 & . & . & . \\ 0 & 3 & 0 & 0 & . & . & . \\ 0 & 0 & 5 & 0 & . & . & . \\ 0 & 0 & 0 & 7 & . & . & . \\ . & . & . & . & . & . & . \\ . & . & . & . & . & . & . \\ . & . & . & . & . & . & . \end{bmatrix}$$

We can write the position and momentum operators in the eigen vector form in terms of raising and lowering operator.

Position operator $\hat{Q}(or\ \hat{X})$

$$\hat{Q} = \sqrt{\frac{\hbar}{2m\omega}}(\hat{a}\dagger + \hat{a}) \quad (18)$$

Momentum operator $\hat{p}$, $\hat{p} = i\sqrt{\frac{\hbar m\omega}{2}}(\hat{a}\dagger - \hat{a})$ (19)

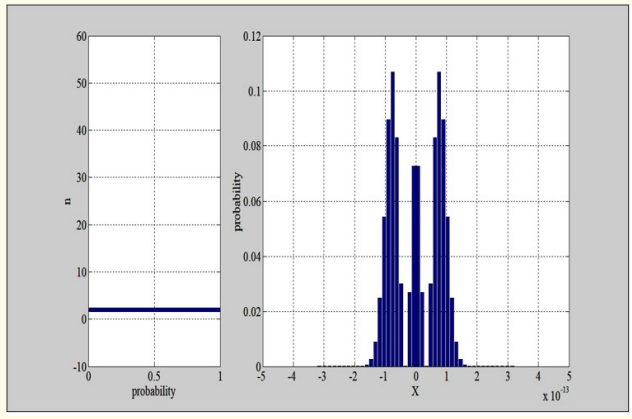

Figure 7: Plot of probability of energy level of Quantum harmonic oscillator in respect to energy level (n=2) and position of the electrons.

Probability of energy states and position of energy eigen values is obsevable in fig. 7. We have plotted this figure using the software Matlab 13.1 whose pseudocodes are available in appendix-2. Left side plot of the figure is showing probability of energy level for a particular values of n (here it is 2nd excited state). Probability distribution in space is ploted in the right side figure. Here Value of N (number of basis states in a truncated representation in quantum harmonic oscillator) is considered to be 50 and n=2 for which we are getting two peaks and one node.

Working sequence of different stages

Following section represents a block diagram in fig. 8 which describe the total detection and treatment of carcinoma comprising of four stages. First stage depicts our main idea of generating X-ray using the principle of quantum harmonic oscillator where suitable levels have to be set. Difference between the quantum numbers of the levels have to be 4,5 or 6. In these three ranges X-ray ($5 \times 10^3 eV$ to 10^4 eV) generation is possible. X-ray crystallography method is the second part of the system for detection of cancerous cells. Next procedure will be placing of gold nanofoils in surrounding of cancerous cells shown in the fig. 11. Gold nanofoils are non reactive to other element and have high contrast compared to other organic substances. Gold NPs does not create any cytotoxicity to human cell found by in vitro observation [19]. Finally appropriate drugs will be delivered to those gold foils to destroy the cancerous cells. Here infrared is mainly used which can transmit readily through human skin and tissues and absorbed by the gold foils. Subsequently the affected cells will be destroyed due to thermal effect.

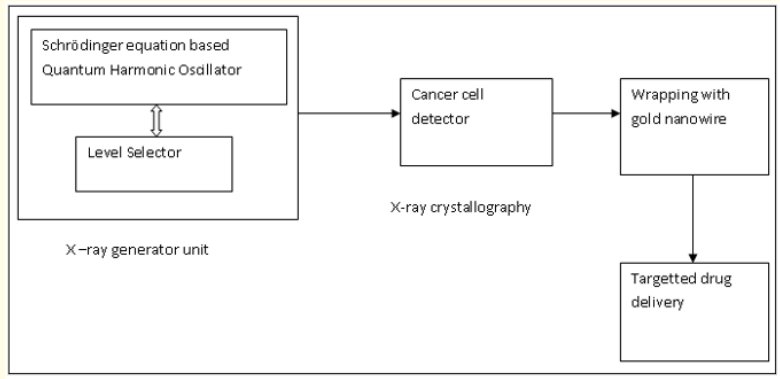

Figure 8: Block diagram of different stages of detection of cancerous cell and its treatment.

X-ray Crystallography is a technique used to ascertain how atoms are arranged in three dimensions within a crystalline solid. We know that the proteins in our body are in the crystal form. When an x-ray strikes a protein it diffracts and forms a pattern shown in fig. 9. By applying Fourier transform we will get the electron density map. Atoms or electrons of gold can then be fitted inside the protein which exactly fit the structure. Suitable drugs is being delivered to cure those affected cells in these gold structures. Interatomic gap of most crystalline minerals is exploited in this technique to create a diffraction gradient for x-ray radiation, which has wavelengths of about 1 angstrom (10^{-8} cm).

A phenomenon called diffraction happens when light comes into contact with an obstruction. If there is a slit, the light waves can either pass through the slits or bend around the obstruction. Areas of constructive interference, or two waves interacting in phase, and destructive interference, or two waves interacting out of phase, will be visible in the ensuing diffraction pattern. The phase difference will be determined by the following Fig. 10:

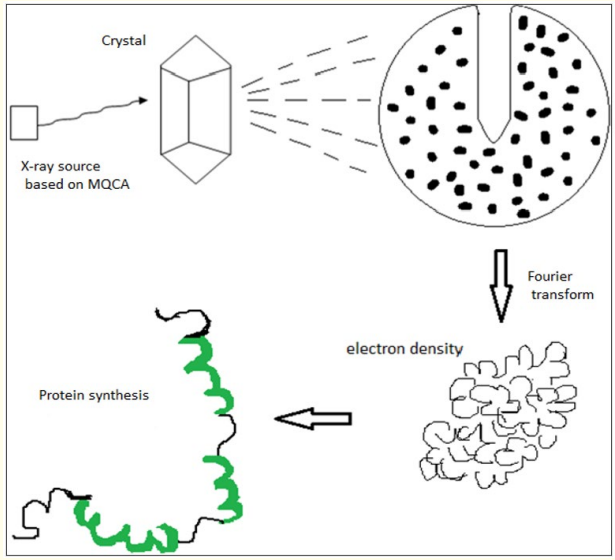

Figure 9: Different steps of incorporation of electron or atom within a protein structure using X- ray crystallography.

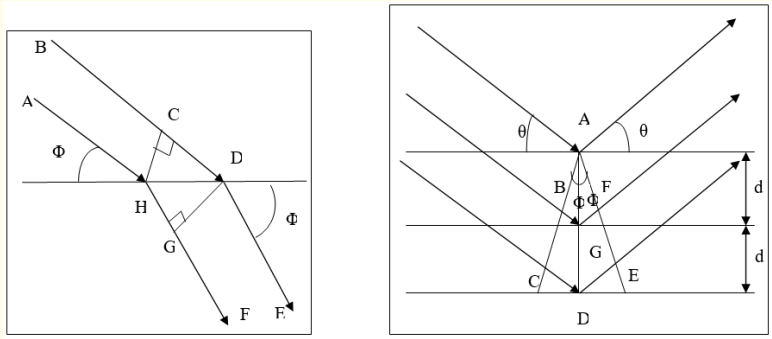

Figure 10: Scattering of light by diffraction gratting.

Here two parallel rays AH and BD are hitting a gradient at an angle of Φ_0. Bd travels more distance than AH by a distance of CD. These rays are scattered as HG and DF respectively at an angle Φ. Here it can be seen that HF covers more distance than DF by a distance of HG. Hence the overall path difference between two rays is CD-HG. In case of high intensity wave,

$CD - HG = n\lambda$, where n = Integer no 1,2, 3.... And λ= wavelength of the light

By trigonometry, $CD = x \cos \Phi_0$ (20)

$HG = x \cos \Phi$, where x = length of HD (21)

Then $(x \cos \Phi - x \cos \Phi_0) = n\lambda$ (22)

When light interacts with the electron cloud encircling the atoms of a crystalline material, diffraction of the X-ray beam takes place. This phenomenon is being shown in fig. 10 where a solid can be characterized as a set of planes with an equal interplaner distance because of its periodic crystalline structure. Some of the light will be diffracted away from the solid at the same angle as the x-ray beam hits the crystal's surface. The remaining light will enter the crystal and interact somewhat with the atoms in the second plane. A portion of the light will penetrate deeper into the solid and be diffracted at an angle Φ. This will be repeated numerous planes in the crystal. After diffraction, the x-ray beams will only interact positively if the path length difference is equal to an integer number of wavelengths since they traverse distinct path lengths before striking the separate planes of the crystal.

Here two diffracted waves will constructively interfere if

$$BG + GF = n\lambda \ , \ BG \ = \ d \sin \Phi$$

$$\text{Therefore, } 2d \sin \Phi \ = \ n\lambda \ (23)$$

Radiation is used in X-rays to produce two-dimensional pictures of inside organs. Greater radiation absorption causes tissues and organs to look white or gray, while less radiation absorption causes materials to seem black. Any abnormal growth in the lung will show up as a somewhat solid area of light gray on a chest X-ray. It could be cancerous development. Small malignancies can occasionally be obscured on an X-ray by bones or the progression of other illnesses like tuberculosis or pneumonia. On an X-ray, cancers that are high in the lungs and on their periphery may be difficult to notice. Additionally frequently overlooked are small tumors and those with a diffuse appearance. Using several X-ray images, a computed tomography scan creates three-dimensional "slices." This facilitates observation of abnormalities in lungs.

The findings of X-ray diffraction tests performed utilizing synchrotron-derived data on hair fibers from breast cancer patients. A novel feature was overlaid on the typical α-keratin diffraction pattern in these patterns. The molecular spacing of the characteristic, which manifested as a ring, was found to be 4.76 ± 0.07 nm. Other standard clinical diagnostic methods evaluated the diffraction patterns of hair from women without breast cancer and found no evidence of this characteristic. Additionally, diffraction patterns from various hairs from the same person that were analyzed on two distinct synchrotron beam lines are very similar.

Targetted drug delivery

Due to their low electrical resistance, gold nanowires (AuNWs) have significant potential applications in plasmonic waveguides and micro and nanoelectronics. Using flexible transfer and solution processing, self-supporting gold nanowire (AuNW) gratings with a thickness of around 50 nm can be created [20]. Still, it is difficult to synthesis pure solvent-dispersible AuNWs with complete control over their length. All the previously published techniques yield AuNWs confined to a specific length (usually less than 10 μm) and with additional impurities such as smaller nanorods, platelets, and spherical particles. The production of extraordinarily long AuNWs (up to 25 μm) with precise control over their dimensions by the use of seed particles which is in the form of pentahedrally twinned gold nanorods (AuNRs) [21]. By adding HCl to the growth fluid, Au (I) was reduced to Au(0) on the surface of AuNRs at a very low pH [22], which caused the AuNW growth.

The length of the AuNWs was proportionate to the amount of Au (I) added to the growth solution, similar to the "living" polymerization reaction. As a result, the required length of AuNWs was obtained by managing the supply of Au(I) ions in the reaction mixture. It was discovered that the AuNWs longer than 6 μm were microwave radiation responsive. Sharp kinks formed in multiple AuNW locations without breaking down into smaller pieces when an aqueous solution of AuNWs was subjected to microwaves.

Large-scale, inexpensive synthesis of Au nanoparticles is feasible for photothermal, intrinsic pharmacodynamic, and cancer medication delivery applications. When chemically functionalized, a 200 nm diameter Au nanoparticle may contain approximately 120,000 different molecules [22, 23]. One of the medicinal drug named DOX is used with Au nanaoparticle for the treatment of breast cell cancer shown in Fig. 12. The structure and function of DOX is also observable from the fig 12.

Figure 11: Gold nanofoil with 10X magnification.

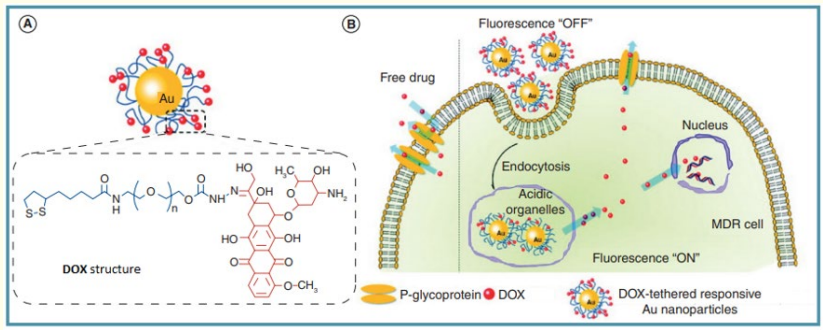

Figure 12: Doxorubicin (DOX) is delivered and internalized by conjugating Au nanoparticles to overcome multi-drug resistance in breast cancer cells. (A) Using an acid-liable poly (ethylene glycol) linker, Au nanoparticles were fictionalized with DOX. (B) After entering the cell via endocytosis, DOX-Au nanoparticles release the conjugated medication into the endo/lysosomal milieu. DOX florescence, which de-quenches when released from the Au nanoparticle, can be used to monitor drug release in this situation, (obtained from [23]).

This is often two to three orders of magnitude more than what liposomes and poly(lactic-co-glycolic acid) nanoparticles can load onto their surfaces. Small compounds, peptides, proteins, nucleic acids (including aptamers), and antibodies (as well as their fragments) can all target the accumulation and intracellular delivery of therapeutic Au nanoparticles. A single change in the number of ligands on an Au nanoparticle's surface can adjust its binding affinity, allowing nanoparticle formulation to be precisely matched to a specific cancer type, stage, or biopsy sample before treatment ever begins. These structures can allow more selective absorption compared to monofunctionalized molecules because of their multivalent avidity, since their sizes are similar to those of cell-surface target receptors.

Discussion

The principle of Quantum Harmonic Oscillator will be a suitable choice for this great method of X-ray generation and its application to various fields along with major implications in medical field. By selecting the suitable frequency range ($1 \times 10^{18} Hz$) and energy levels (11 and 12) X-ray generation is possible. Here very low power in the range of only 3-5 mW is enough for generation. X-ray crys-

tallography method is used for detection of cancerous cells followed by placing of gold nanofoils in surrounding of cancerous cells. Gold nanofoils (AuNW) have several special qualities that make them ideal for messing with cancer cells. These include their non-reactivity to other elements, high contrast when compared to other organic compounds, and non-cytotoxicity to human cells. At last, the right medications will be administered to those gold foils in order to eradicate the malignant cells. Here, the primary radiation used is infrared, which is easily absorbed by gold foils and transmits through human skin and tissues. The afflicted cells will thereafter be destroyed as a result of the heat impact.

We have drawn the graphs of energy analysis of QHO using Matlab 13.1 software. Origin pro 2024 software make it possible to draw polarisation of cells in Molecular QCA with relation to temperature in Kelvin scale. As a whole this work will be socially beneficial for improvement in cancer treatment.

Conclusions

We have presented a brand-new QHO-based X-ray generation design that is exceptional because of its consistent difference in subsequent energy levels. We have also observed that it operates effectively at room temperature without experiencing any polarization failures. This is utilized to mesh with a gold nanowire to detect cancer in breast and lung cells, and then to start treatment with targeted drug delivery. The produced X-ray has a very low power consumption and can be used in a wide range of industrial applications, such as detecting metal cracks and verifying the purity of chemicals.

References

1. S Prabhu., et al. "Production of X-RAYS using X-RAY Tube". Journal of Physics.: Conf. Ser 1712 (2020): 012036,
2. CG Camara, JV Escobar and JRHSJ Putterman. "Correlation between nanosecond x-ray flashes and stick-slip friction in peeling tape". NATURE 445.7216 (2008): 1089-1092.
3. B Jerrold., et al. "The essential physics of medical imaging". Lippincott Williams & Wilkins 72.17 (2002): 116.
4. RM Polichar, RC Schirato and J Baltgalvis. "Portable, digital x-ray apparatus for producing, storing, and displaying electronic radioscopic images". US patent- US 7, 289 (2007): 602 B1.
5. Duerr Martin Kimutai. "Structured electron emitter for coded source imaging with an x-ray tube". US patent- US-20120027173-A1 (2012).
6. Tolt Zhidan Li. "Low voltage electron source with self aligned gate apertures, fabrication method thereof, and x-ray generator using the electron source". US patent- US-20120219118-A1 (2012).
7. Molloi Sabee., et al. "Tio2 nanotube cathode for X-Ray generation". US patent-US-20110280371-A1 (2011).
8. Behling Rolf Karl Otto. "X-ray generating device with electron scattering element and x-ray system". US patent-US-20120207269-A1 (2012).
9. Tougaw PD and Lent CS. "Logical devices implemented using quantum cellular automata". J Appl Phys 75 (1994): 1818-1825.
10. F Karim, K Walus and A Ivanov. "Analysis of field-driven clocking for molecular quantum-dot cellular automata based circuits". J Comput Electron, vol. 9, (2010): 16-30.
11. "Harmonic oscillator Notes on Quantum Mechanics". Department of Chemistry, Boston University, Boston MA (2006): 02215.
12. Ardesi Y., et al. "M. Impact of molecular electrostatics on field-coupled nanocomputing and quantum-dot cellular automata circuits". Electronics 11 (2022): 276.
13. G Beretta., et al. "Multi-Molecule Field-Coupled Nanocomputing for the Implementation of a Neuron". in IEEE Transactions on Nanotechnology 21 (2022): 52-59.
14. Ardesi Y., et al. "Effectiveness of Molecules for Quantum Cellular Automata as Computing Devices". J. Low Power Electron. Appl 8 (2018): 24.
15. Ardesi Y., et al. "Ab initio molecular dynamics simulations of field-coupled nanocomputing molecules". j. integr. Circuits syst 16 (2021): 1-8.

16. Y Wang and M Lieberman. "Thermodynamic behavior of molecular-scale quantum-dot cellular automata (qca) wires and logic devices". IEEE transactions on nanotechnology 3.3 (2004).
17. AJF Levi. "Applied Quantum Physics". 2nd edition, Cambridge University Press (2006).
18. Paramartha Dutta and Debarka Mukhopadhyay. "An Ultra Low Power Molecular Quantum Dot Cellular Automata Based X-ray (QX-ray) Generating System Using Renewable Energy Source". Encyclopedia of Renewable and Sustainable Materials, Elsevier (2020): 810-820.
19. Vales G., et al. "Size, Surface Functionalization, and Genotoxicity of Gold Nanoparticles In Vitro". Nanomaterials (Basel) 10.2 (2020): 271.
20. Xia Q., et al. "The Effect of Particle Size on the Genotoxicity of Gold Nanoparticles". J. Biomed. Mater. Res. A (2017).
21. Bishnu P Khanal and Eugene R Zubarev. "Gold Nanowires from Nanorods". Langmuir 36.49 (2020): 15030-15038.
22. Jinghui Yang., et al. "A self-supported ultrathin plasmonic film for ultrafast optical". Nanoscale Adv 4 (2022): 943.
23. Dreaden EC., et al. "Size matters: gold nanoparticles in targeted cancer drug delivery". Therapeutic Delivery 3.4 (2012): 457-478.

Appendix 1

Pseudocode of first 5 eigenstates within zero potential well:

```
#Apply degeneracy

N=100; #Jacobian Laplacian function for derivatives

x=0:N-1; # Dimensions of laplacian function

#Laplacian function NxN with non zero diagonals and off diagonals

Lap = (-2*diag(ones(N,1),0) + diag(ones((N-1),1),1) ...

+ diag(ones((N-1),1),-1)); #modify Lap so that it is consistent with f(0) = f(L) = 0

Lap(1,1) = 0; Lap(1,2) = 0; Lap(2,1) = 0;

Lap(N,N-1) = 0; Lap(N-1,N) = 0; Lap(N,N) = 0;

#Define Hamiltonian for the system of QHO

#find eigensolutions to Hamiltonian matrix eigenenergies and eigenvectors

[V,E]=eig(H); #E given as square matrix with values on diagonal ,diagonalise for eigenenergies

En=diag(E);

#compare with normalised eigenstates

sqrt(2/L)*sin((10.*pi.*x)/L)';
```

Appendix 2

Pseudo code for energy level generation of quantum harmonic oscillator

```
#Assign constants

#Define parameters like number of basis states in truncated representation of QHO, oscillator frequency, angular oscillator frequency etc.

#Next step-calculation
```

```
#Construct operators for the QHO

a=diag(sqrt(1:N-1),1); #lowering operator in energy basis

ad=a′; #raising operator in energy basis

H-hbar*w*(ad*a+0.5.*eye(N));

X=sqrt(hbar/2*m*a))*(ad+a);

#Define index for an eigenstate

#Create transform matrix of energy to site basis #Plot in bar form.
```

Volume 7 Issue 3 September 2024